HHS Public Access

Author manuscript

Nanomedicine. Author manuscript; available in PMC 2016 January 01.

Published in final edited form as:

Nanomedicine. 2015 January ; 11(1): 195–206. doi:10.1016/j.nano.2014.09.004.

Curcumin-encapsulated nanoparticles as innovative antimicrobial and wound healing agent

Aimee E. Krausz, BA[1,*], **Brandon L. Adler, BA**[1,*], **Vitor Cabral, PhD**[2], **Mahantesh Navati, PhD**[3], **Jessica Doerner, MS**[2], **Rabab Charafeddine, MSc**[3], **Dinesh Chandra, PhD**[2], **Hongying Liang**[3], **Leslie Gunther, MSc**[4], **Alicea Clendaniel, BS**[5], **Stacey Harper, PhD**[5,6], **Joel M. Friedman, PhD**[3], **Joshua D. Nosanchuk, MD**[2], and **Adam J. Friedman, MD**[1,3]

[1]Division of Dermatology, Department of Medicine, Albert Einstein College of Medicine, Bronx, New York, USA

[2]Department of Microbiology & Immunology, Albert Einstein College of Medicine, Bronx, New York, USA

[3]Department of Physiology and Biophysics, Albert Einstein College of Medicine, Bronx, New York, USA

[4]Analytical Imaging Facility, Albert Einstein College of Medicine, Bronx, New York, USA

[5]Department of Environmental and Molecular Toxicology, Oregon State University, Corvallis, Oregon, USA

[6]School of Chemical, Biological and Environmental Engineering, Oregon State University, Corvallis, Oregon, USA

Abstract

Burn wounds are often complicated by bacterial infection, contributing to morbidity and mortality. Agents commonly used to treat burn wound infection are limited by toxicity, incomplete microbial coverage, inadequate penetration, and rising resistance. Curcumin is a naturally derived substance with innate antimicrobial and wound healing properties. Acting by multiple mechanisms, curcumin is less likely than current antibiotics to select for resistant bacteria. Curcumin's poor aqueous solubility and rapid degradation profile hinder usage; nanoparticle encapsulation overcomes this pitfall and enables extended topical delivery of curcumin. In this study, we synthesized and characterized curcumin nanoparticles (curc-np), which inhibited *in vitro* growth of methicillin-resistant *Staphylococcus aureus* (MRSA) and *Pseudomonas aeruginosa* in dose-dependent fashion, and inhibited MRSA growth and enhanced wound healing in an *in vivo* murine

Corresponding author: Adam J. Friedman, MD, Division of Dermatology, Montefiore Medical Center, 111 E. 210th Street, Bronx, NY 10467, adfriedm@montefiore.org, Phone: 718-920-2680/Fax: 718-944-4219.

*These authors contributed equally to this work.

Abstract previously presented at: 72nd Annual Meeting of the American Academy of Dermatology; 2014 Mar 21-25; Denver, CO

Conflict of interest: None of the authors have any conflict of interest to declare

wound model. Curc-np may represent a novel topical antimicrobial and wound healing adjuvant for infected burn wounds and other cutaneous injuries.

Graphical abstract

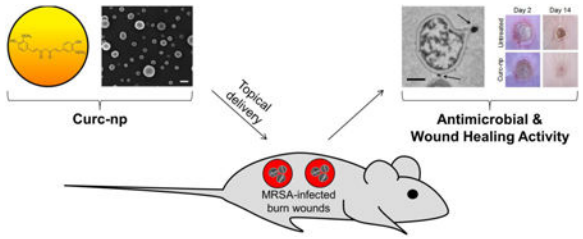

Curcumin was encapsulated into a silane-hydrogel nanoparticle vehicle (curc-np) to overcome native curcumin's poor solubility and investigate its potential as a topical therapy for wound infection. Curc-np demonstrated efficacy *in vitro* against methicillin-resistant *Staphylococcus aureus* (MRSA), and inhibited MRSA growth and enhanced wound healing in an *in vivo* murine full-thickness burn wound model. These data suggest that curc-np may possess clinical utility as a novel topical antimicrobial and wound healing agent for infected burn wounds.

Keywords

curcumin; nanoparticle; burn wound; wound healing; infection; antimicrobial

Background

Among traumatic injuries, burns represent a significant source of morbidity and mortality.[1] The avascular wound bed provides an ideal environment for microbial growth, facilitating penetration of pathogens into underlying tissue, with potential for hematogenous dissemination.[2] Up to 75% of deaths following burn injury relate to infection,[3] most commonly caused by methicillin-resistant *Staphylococcus aureus* (MRSA) and *Pseudomonas aeruginosa*.[1] Currently employed antimicrobial agents possess limited utility due to toxicity, incomplete antimicrobial coverage, inadequate wound bed penetration, and growing bacterial resistance.[1] In addition, mainline treatments such as silver sulfadiazine (SS) may delay burn wound healing.[4]

Curcumin (diferuloylmethane) is a yellow crystalline compound and the active ingredient of turmeric, a traditional Asian spice, cosmetic, and folk remedy.[5] Over the last century, curcumin has been found to possess antineoplastic,[6] antimicrobial,[7] anti-inflammatory,[8] antioxidant,[9] and wound healing activities.[10] Given its numerous therapeutic targets, curcumin has been piloted in clinical trials for myriad disease entities, with oral doses as high as 12 grams per day tolerated safely.[11] However, curcumin's potential for therapeutic translation has been hindered by low oral bioavailability, poor aqueous solubility, and rapid degradation, restricting clinical applicability.[12]

Encapsulation of curcumin in a nanoparticle platform is a feasible and advantageous means of enabling its delivery. By virtue of their small size and high surface-to-volume ratio,

nanoparticles can pass through the skin barrier and intracellularly,[12] ideal for topical drug delivery. Slow, sustained release of encapsulated contents limits toxicity as the theoretical maximum amount of drug is never in contact with skin at one time. Of considerable interest within our study, nanoparticles make possible the delivery of substances such as curcumin with physicochemical properties that prohibit or retard their use in non-encapsulated form. Curcumin nanoformulations have been developed for preclinical studies on cancer, inflammation, wound healing, and other conditions, which demonstrate enhanced therapeutic efficacy with nano-versus non-encapsulated curcumin[12,13]; however, limited data exists within the infection landscape,[14] with no *in vivo* studies published to date.

In an attempt to further improve curcumin delivery, we utilized an innovative sol-gel-based polymerization technique to create silane composite nanoparticles that incorporate curcumin within a highly structured porous lattice.[15] Sol-gel technology offers discrete advantages over other nanoplatforms, with greater drug loading capacity than liposomes[16] and easily modifiable characteristics.[17] For instance, pore size distribution can be changed to alter release rate of encapsulated drug.[18] Sol-gel technology is also cost effective, biocompatible, and nontoxic.[17] Our platform has been employed to encapsulate agents ranging from nitric oxide for infection and wound healing[15,19] to amphotericin B for fungal burn wound infections[20] to sildenafil for erectile dysfunction.[21] The versatility of our nanoformulation allows for loading of different active ingredients, with therapeutic efficacy when applied topically, intradermally, and intravenously.[19,22,23] We hypothesized that this fabrication strategy would allow for the encapsulation and continuous release of curcumin, with activity in the setting of infected burn wounds.

Methods

Clinical isolates

Clinical isolates were collected from patients' wounds at Montefiore Medical Center (Bronx, NY) and obtained with written patient consent according to standards of the institutional review board at Albert Einstein College of Medicine. Studies were conducted according to Declaration of Helsinki principles. Twelve clinical isolates were evaluated, including 8 MRSA and 4 *P. aeruginosa* strains, and stored at 4° C on tryptic soy agar (TSA).

Synthesis of curc-np

To create curc-np, we modified our previously described sol-gel-based protocol.[15] Tetramethyl orthosilicate (TMOS) was hydrolyzed by adding HCl, followed by 20-minute sonication in ice bath. The mixture was refrigerated at 4° C until monophasic. Curcumin (Sigma-Aldrich, St. Louis, MO, USA, mol wt 368.38) was dissolved in methanol and combined with chitosan (4.4%, 5 mg/ml), polyethylene glycol 400 (PEG400; 4.4%, avg mol wt 400), and TMOS-HCl (8.8%) to induce polymerization. The gel was lyophilized at ∼200 mTorr for 48-72 hours, removing all traces of methanol. The resulting powder was processed in a ball mill for ten 30-minute cycles to achieve smaller size and uniform distribution. Results were consistently reproducible. Control nanoparticles were synthesized identically to curc-np, without addition of curcumin.

Scanning electron microscopy

Nanoparticles were plated on poly-L-lysine-coated coverslips, critical point dried using liquid CO_2 in Samdri-795 Critical Point Dryer (Tousimis, Rockville, MD), and sputter coated with chromium in Q150T ES Sputter Coater (Quorum Technologies Ltd, East Sussex, UK). Samples were examined under Supra Field Emission Scanning Electron Microscope (Carl Zeiss Microscopy, Peabody, MA) with 3 kV accelerating voltage.

Dynamic light scattering

Curc-np suspension (1 mg/ml) was sonicated in distilled water, and size was measured using DynaPro NanoStar (Wyatt Technology, Santa Barbara, CA). Experiments were conducted in triplicate, with 40 acquisition attempts (acquisition length 5 seconds) per sample. Average nanoparticle hydrodynamic diameter and polydispersity index were calculated from results.

In vitro release kinetics

Amount of encapsulated curcumin was evaluated by comparing spectrophotometric absorbance of curc-np dissolved in methanol to standard curve of curcumin using Lambda 2 UV/VIS spectrometer (PerkinElmer, Waltham, MA). Release over time was evaluated by dispersing individual aliquots of 2 mg/ml curc-np (n=4 per time point) in phosphate buffered saline (PBS, pH=7.4) and incubating at 37° C at 100 rpm using innova 2300 platform shaker (New Brunswick Scientific, Enfield, CT). At 2-hour intervals, individual samples were pelleted and dissolved in methanol to solubilize unreleased curcumin. The amount released was calculated by dividing absorbance at each time point by absorbance of the estimated encapsulated maximum.

Cellular cytotoxicity assay

Using the semiquantitative FDA (fluorescein diacetate) metabolic assay, susceptibility of murine PAM212 keratinocytes to curc-np was assessed. 2×10^4 keratinocytes were plated in a 96-well plate and grown overnight in Dulbecco's modified Eagle's medium (DMEM) containing 10% fetal bovine serum, 1% HEPES, 1% nonessential amino acids, and 1% penicillin-streptomycin. Cells were incubated with 200 μl of media containing curc-np 5 mg/ml for 24 hours at 37° C, 5% CO_2. Metabolic activity was measured by FDA assay[24] and statistical analysis conducted using Student's *t*-test.

Zebrafish cytotoxicity assay

Zebrafish embryos (*Danio rerio*, wild type, 5D-Tropical strain) were obtained from Sinnhuber Aquatic Research Laboratory, Oregon State University. Exposures and evaluations were conducted according to Truong *et al*.[25] Curc-np were dispersed in fish water at stock concentration of 1000 ppm prior to serial dilutions. Embryos were dechorionated at 6 hours post-fertilization (hpf) by pronase enzyme degradation and at 8 hpf were transferred to 96-well plates, one embryo per well (n=24). Plates were incubated at 26.5° C under a photoperiod of 14:10 hour light:dark cycle. Effects were evaluated in binary notation as either present or not present. Statistical analysis was performed using Fisher's exact test at $p \leq 0.05$ for each endpoint.

Susceptibility of bacterial strains to curc-np

For each strain, 1 μl aliquots of known bacterial suspension were transferred to 100-well honeycomb plates with 199 μl TSB, containing 5 and 10 mg/ml of curc-np and control np. Based on spectrophotometric release calculations, an equivalent concentration of free curcumin (50 and 100 μg/ml) dissolved in 4% DMSO was used as comparative control. DMSO (4%) was evaluated independently. Background absorbance of each concentration was accounted for by wells containing nanoparticles and TSB alone. Optical density readings were acquired at 600 nm hourly for 24 hours using a microplate reader (Bioscreen C, Growth Curves USA, Piscataway, NJ). Statistical significance of growth was assessed by 2-way ANOVA.

Colony forming unit (CFU) quantification was performed on MRSA and *P. aeruginosa* isolates to determine antimicrobial activity of curc-np. A suspension of 10^7 cells was incubated with 1.0 ml of DMEM (Mediatech, Herndon, VA) containing curc-np (5 and 10 mg/ml), and compared to untreated control, control np (5 and 10 mg/ml), curc (50 and 100 μg/ml in 4% DMSO in DMEM) and DMSO (4% in DMEM). Tubes were incubated at 37° C for 4 hours using a tube rotator (ATR, Laurel, MD) to ensure uniform distribution. After incubation, suspensions were serially diluted in PBS, plated onto TSA and incubated for 24 hours at 37° C under aerobic conditions. Individual colonies were counted and number of CFUs tabulated. Statistical significance of growth was assessed by 1-way ANOVA.

Transmission electron microscopy

A suspension of 5×10^8 MRSA cells was incubated for 6 and 24 hours with and without 5 mg/ml of control np and curc-np. Samples were fixed with 4.0% paraformaldehyde and 5% glutaraldehyde in 0.2 M sodium cacodylate buffer mixed 1:1 with serum-free media, enrobed in 3% gelatin, postfixed with 1% osmium tetroxide followed by 1% uranyl acetate, dehydrated through a graded series of ethanol and embedded in Spurrs resin (Electron Microscopy Sciences, Hatfield, PA). Ultrathin sections were cut on Reichert Ultracut UCT, stained with uranyl acetate followed by lead citrate and viewed on 1200EX transmission electron microscope (TEM; JEOL, Peabody, MA) at 80 kV.

In vivo infected murine burn model

All procedures for animal experimentation were approved by the Institutional Animal Care and Use Committee at Albert Einstein College of Medicine. Dorsal hair of Balb/c mice (6–8 weeks; National Cancer Institute, Frederick, MD) was shaved, and full-thickness 5-mm diameter burn injuries were created by applying a calibrated 160° C heated bar to the backs for 10 seconds (n=10 wounds per group). A suspension of MRSA containing 5×10^8 cells was inoculated onto each wound. All treatments were prepared in melted coconut oil (CO), which solidified in syringes. Treatment groups included untreated control, CO (delivery control), control np, curc, and curc-np. The concentration of curcumin delivered was 7.5 mg/ml in both curc and curc-np groups. Beginning 24 hours after infection, 50 μl of treatment was applied topically without occlusion once daily for 7 days. Wound tissue was excised on days 3 and 7, homogenized in 10 ml of PBS, serially diluted, and plated onto TSA. CFUs were quantified and analyzed for statistical significance using 1-way ANOVA.

In vivo murine burn model

Burn wounds were created on Balb/c mice (n=10 wounds per group) and treatment administered daily as detailed above starting on the day of wounding. Treatment groups included untreated control, SS, control np, curc, and curc-np. CO was used as delivery vehicle for all treatment groups except SS, and was evaluated independently. Daily photographs were taken and change in wound area relative to initial area was calculated using ImageJ software (National Institutes of Health, Bethesda, MD), with statistical significance determined by 2-way ANOVA. On day 13, wounds were excised, fixed in 10% formalin, and embedded in paraffin. Four-micron vertical sections were stained with hematoxylin and eosin (H&E), Masson's trichrome, and CD34 to observe morphology, collagen deposition, and angiogenesis (microvessels), respectively. Slides were observed under light microscopy and images were captured without further processing. Slides were numbered without indication of cohort to blind interpretation. Collagen deposition was measured by intensity using ImageJ. Ten HPFs (40×) were evaluated per section and analyzed for statistical significance using 1-way ANOVA.

In vitro keratinocyte migration assay

Murine PAM212 keratinocytes were seeded in 6-well plates and grown until confluent. Four scratches were applied per well using 200 μl pipette tips prior to incubation with and without 0.5 mg/ml curc-np. Cell migration over 24 hours was imaged by time-lapse microscopy at 2-hour intervals in environmental chamber using 4D spinning-disk confocal microscope (PerkinElmer, Waltham, MA) with 10× objective and Orca ER digital camera (Hamamatsu, Bridgewater, NJ). Statistical analysis was conducted using Student's *t*-test.

Results

Characterization of curc-np

Scanning electron microscopy revealed distinct spherical nanoparticles with irregular surface structure indicative of the porous matrix lattice (Figure 1A). Dynamic light scattering showed a narrow size range with average hydrodynamic diameter of 222 ± 14 nm (Figure 1B), likely an overestimate as nanoparticles swell with moisture. The total theoretical amount of encapsulated curcumin per mg of particle was calculated to be 10 μg. Release occurred in a controlled and sustained manner, with incomplete release of the calculated maximum after 24 hours (Figure 1C). In the first 6 hours, 42.3% of curcumin was released, increasing to 81.5% after 24 hours, amounting to a total release of 8.15 μg per mg of particle (e.g., 1 mg/ml curc-np = 8.15 μg/ml curcumin). Our results therefore indicate that complete release of encapsulated curcumin does not occur, and the therapeutic efficacy observed throughout this study occurred at concentrations less than calculated theoretical maximum doses.

Cytotoxicity studies of curc-np *in vitro* and *in vivo*

The effect of curc-np on viability of PAM212 keratinocytes was measured by FDA assay. Cells treated with curc-np 5 mg/ml exhibited 81.7% cell viability as compared to untreated control ($p \leq 0.005$, Supplementary Figure 1S). *In vivo* toxicological impact of curc-np was

assessed via embryonic zebrafish assay (Figure 1D-E). At 24 hours post-fertilization, embryos were examined for mortality, developmental progression, notochord development, and spontaneous movement. At 120 hpf, larval morphology and behavior were examined. Body axis, eye, snout, jaw, otic vesicle, heart, brain, somite, pectoral fin, caudal fin, yolk sac, trunk, circulation, pigment, and swim bladder malformations were recorded, as well as motility and tactile response. Exposure to curc-np did not elicit any toxic responses after 5 days of exposure during a sensitive developmental time period. No statistical differences were appreciated from fish water control with respect to mortality, development, larval morphology, or behavioral endpoints.

Curc-np inhibit planktonic growth of Gram-positive and -negative organisms

Due to the incidence of MRSA and *P. aeruginosa* infection in burn wounds, the activity of curcnp against these species was evaluated *in vitro* (Figure 2). For MRSA (Figure 2A), curc-np exhibited a significant antimicrobial effect from t=8 hours onward in comparison to both untreated control and control np ($p \leq 0.0001$). Control np did not exhibit significant activity compared to untreated control ($p > 0.05$). Both curc in DMSO and DMSO control completely inhibited MRSA growth and were significant against all other groups ($p \leq 0.0001$); therefore, due to the high concentration of DMSO required for curcumin solubilization, it was not possible to characterize the antimicrobial efficacy of free curcumin. For *P. aeruginosa* (Figure 2B), curc-np exhibited a significant effect against control np ($p \leq 0.05$) and untreated control ($p \leq 0.0001$) from t=8 hours onward. Both curc in DMSO and DMSO control completely inhibited *P. aeruginosa* growth. The growth inhibition exhibited by control nanoparticles is consistent with prior studies conducted using this technology and can be attributed to the physical presence of particles, which interferes with cell-cell interactions, and intrinsic properties of nanoparticle components, e.g., chitosan.[19,26] However, the significantly greater activity of curc-np as compared to control np highlights curcumin's independent antimicrobial effects, notably more active against MRSA compared to *P. aeruginosa*.

CFU quantification showed that curc-np exerted a 97.0% reduction of MRSA growth (Figure 2C) and 59.2% reduction of *P. aeruginosa* growth (Figure 2D), significant compared to both untreated control and control np ($p \leq 0.0001$). Curc did not differ significantly from curc-np for MRSA isolates, but was significant for *P. aeruginosa* isolates ($p < 0.05$).

Curc-np disrupt MRSA cellular architecture

In an effort to explore the mode of action of curc-np's antimicrobial activity, MRSA incubated with curc-np and control np was assessed over time by TEM (Figure 3). Untreated MRSA (Figure 3A) showed intact cellular architecture with uniform cytoplasmic density and highly contrasting cross wall. After 24 hours, MRSA incubated with control np did not exhibit changes in cellular architecture compared to untreated control despite visible interaction with nanoparticles (Figure 3B). In contrast, 6 hours after treatment with curc-np (Figure 3C), MRSA cells displayed edema and distortion in association with particles contacting the cell wall, with subsequent lysis and extrusion of contents after 24 hours (Figure 3D).

Curc-np reduce bacterial burden in MRSA-infected burn wounds

Antimicrobial activity of curc-np against MRSA was evaluated *in vivo* by homogenizing infected burn wounds and quantifying CFUs present in tissue on day 3 (Figure 4A) and day 7 (Figure 4B). Curc-np-treated wounds showed statistically significant reductions in bacterial counts on both days compared to untreated infected control, CO, control np and curc-treated wounds ($p \leq 0.0001$). Control np, CO, and curc did not differ significantly from each other on either day ($p > 0.05$). All groups were significant compared to untreated control on day 7 ($p \leq 0.0001$). Independent antimicrobial effects can be attributed to CO, as shown previously,[27] but were significantly enhanced by addition of curc-np.

Curc-np accelerate wound healing in murine burn model

Topical administration of curc-np significantly accelerated wound healing in mice as compared to untreated control, CO, SS, control np and curc groups ($p \leq 0.0001$, Figure 5). Burn wounds demonstrate an expanding zone of inflammation in early stages post-injury, corresponding to progressive tissue loss. Curc-np mitigated the observed wound expansion, and on day 4 curc-np-treated wounds measured 98.1 ± 4.4% compared to day 0, in contrast to size increases in untreated control (132.9 ± 4.3%), CO (153.0 ± 4.04%), SS (127.5 ± 13.2%), control np (124.7 ± 4.41%), curc (118.0± 2.6%). In addition to accelerated closure, qualitative assessment demonstrated that curc-np-treated wounds displayed more well-formed granulation tissue and reepithelialized earlier than other groups (Figure 5B).

Curc-np enhance granulation tissue formation, collagen deposition, and new vessel formation

Histologic evaluation of wound sections from day 13 revealed distinct differences in maturity of the epidermis/dermis and quality of granulation tissue between curc-np and other groups (Figure 6A). Both curc and curc-np demonstrated accelerated maturation and a well formed epidermis with compact orthokeratosis, while other groups displayed more inflammatory granulation tissue and partially re-epithelialized epidermis with overlying serum crust. When comparing curc to curc-np, the greatest difference was appreciated in the dermis, where the curc-treated wounds contained a subjectively greater degree of mixed inflammatory infiltrate splaying between both degenerated and newly formed collagen as compared to curc-np-treated groups.

Evaluating collagen deposition, untreated control, SS, and control np displayed pale, necrotic, haphazardly deposited immature collagen (Figure 6B). Curc-treated wounds demonstrated pale but more mature collagen bundles than aforementioned controls. In contrast, curc-np-treated wounds displayed well-organized compact collagen bundles that were oriented parallel to the epidermis. Furthermore, trichrome semi-quantitative analysis revealed significantly increased collagen intensity (in arbitrary units, A.U.) in curc-np-treated wounds compared to all other wounds ($p \leq 0.0001$; Figure 6B).

New vessel formation, a hallmark of the proliferative phase of healing, was evaluated using CD34 staining. There was significantly greater neovascularization in wounds treated with curcnp compared to all other groups ($p \leq 0.0001$; Figure 6C), determined by number of stained microvessels per high-power field (HPF; 40×; 10 fields).

Curc-np do not influence keratinocyte migration

To explore a potential mechanism of curc-np in wound healing, keratinocyte cellular migration assay was performed. No significant difference in relative wound area or migration rate was observed between untreated, control np and curc-np-treated keratinocytes at 12 or 24 hours post-administration of scratch to cell monolayer (Supplementary Figure 2S).

Discussion

In this study, we demonstrate curc-np's antimicrobial and healing efficacy in the setting of burn wounds using a unique sol-gel-based formulation. We expand on previous work employing diverse curcumin nanoformulations for antimicrobial[14,28] and wound healing purposes[13,29] by providing the first *in vivo* curcumin nanoparticle data in the setting of skin infection. No previous study evaluated both antimicrobial and wound healing capabilities of a single curcumin nanoplatform, limiting the clinical translatability of those findings. Furthermore, the data presented recapitulate the utility of the embryonic zebrafish model to study skin pathology and comment on its physiologic relevance to humans as suggested by previous investigators.[30]

Sol-gel processing is a wet-chemical technique consisting of hydrolysis and polycondensation in which the “sol” (solution) gradually evolves toward formation of a gel-like system, with subsequent removal of the solvent phase through a drying process. Metal alkoxide precursors (TMOS) polymerize into a highly structured porous lattice consisting of siloxane bonds.[17] Incorporation of PEG and chitosan forms a strong glass-like hydrogen bonding network that “plugs” the pores of the sol-gel, inhibiting rapid release. Upon aqueous exposure, disruption of this hydrogen bonding network leads to extended release of trapped drug.[15] PEG controls pore size in the sol-gel matrix, and thus is the primary effector of release characteristics.[16] We selected PEG400 as prior experiments showed slower, more sustained release with incorporation of lower molecular weight PEG.[15]

Nano-incorporation of curcumin overcomes the challenges posed by its insolubility in aqueous media and rapid degradation kinetics. Although curcumin is soluble in DMSO, this solvent is only approved by the FDA for intravesical administration. In our *in vitro* antimicrobial assays, fully solubilizing the amount of curcumin needed required DMSO concentrations that proved cytotoxic. In our *in vivo* experiments, we utilized coconut oil rather than DMSO as the delivery vehicle in order to avoid this toxicity. The *in vivo* antimicrobial and wound healing capabilities of curc-np were significantly greater than those of free curcumin. This is likely related in part to the small size and high surface-to-volume ratio of nanoparticles, facilitating enhanced passage through biological barriers, as well as increasing desired interactions with host cells and microbial pathogens.[12] Not insignificantly, the readily apparent orange skin discoloration produced by application of free curcumin was avoided with nanoencapsulated curcumin, eliminating a potential cosmetic concern associated with topical curcumin use and enhancing clinical translatability of this substance.

The antimicrobial activity of curcumin is incompletely characterized but by interacting with numerous molecular targets and transduction pathways,[31] it employs a multi-mechanistic anti-infective strategy. This contrasts with currently used antibiotics, which act by one or a few mechanisms, and are therefore susceptible to microbial resistance mechanisms. Curcumin has been shown to inhibit cellular proteins FtsZ[32] and sortase A,[33] thereby interrupting cytokinesis and cellular adhesion, and interfere with biofilm formation.[34] Though curcumin exhibits broad antimicrobial activity, our data suggest that Gram-positive species are more susceptible than Gram-negatives, as observed in other studies.[14,28] We believe this relates to differences in cell membrane charge and composition, resulting in decreased nanoparticle interaction with Gram-negative cells. Imaging of MRSA cells in the presence of curc-np clearly demonstrated interaction of nanoparticles with the cellular membrane, resulting in progressive edema and lysis of cells, as shown previously.[14] Encapsulation in a nanoscale carrier extends the inherent antimicrobial properties of curcumin by facilitating interaction with pathogen surfaces unattainable by free curcumin.[12]

As with its antimicrobial action, curcumin's impact on wound healing is multifaceted. Wound healing is a complex and dynamic process divided into phases of inflammation, proliferation, and maturation. Curcumin has been found to primarily act in the proliferative phase by increasing re-epithelialization,[35] collagen deposition,[10,35,36] fibronectin production,[35] and myofibroblast contraction.[35] These findings may be mediated by effects on TGF-β1 and inducible nitric oxide synthase,[36] as well as antioxidant[37] and anti-inflammatory activities.[38] In line with previous studies, on histologic analysis we observed enhanced granulation tissue formation, with greater collagen proliferation, maturity, and organization as well as increased neovascularization in curc-np-treated compared to other groups, though free curcumin in CO did demonstrate a superior effect to other control groups. We observed no effect of curc-np on keratinocyte migration, in congruence with past investigations using fibroblasts,[39] confirming our belief that curcumin acts via proliferative rather than cellular migratory effects. Although curcumin is associated with decreased angiogenesis in the setting of cancer, enhanced neovascularization has been reported with use of curcumin in wound healing, and may relate to effects on nitric oxide synthase.[36] Notably, silver sulfadiazine, the gold standard for topical burn therapy, did not outperform even untreated control, suggesting that re-evaluation of this commonly used therapy may be warranted.[4] This also highlights the need for new agents like curc-np that provide antimicrobial coverage while simultaneously reducing healing time.

In developing a topical antimicrobial and wound healing agent, a favorable adverse effect profile is essential for therapeutic translation. Toxicity of nanomaterials is a common concern. While topical application of various nanoparticle formulations has not been associated with significant toxic effects or systemic absorption,[40,41] compromise of the skin barrier (e.g., in the setting of acute or chronic wounds) may permit systemic absorption and internal organ accumulation of nanomaterials. We have consistently shown a lack of toxicity following topical as well as systemic administration of our nanoparticles.[19,22] This is reflected clinically as well as histologically in the current study, in which wounds treated with curc-np demonstrated well-organized granulation tissue without evidence of increased inflammation or necrosis. Our synthetic protocol utilized methanol prior to gel formation,

but complete drying of particles eliminated methanol from the final product. Reported *in vitro* toxicity of curcumin (free and in nanoparticle form) ranges from no toxicity[13,42] to dose-dependent toxicity in normal cells,[43,44] with selectivity for cancer cells compared to normal cells.[43,45] Our finding of 81.7% viability at 24 hours falls within the range of reported viabilities (60 to over 90%) at comparable concentrations.[13,43-46] As cell culture studies do not accurately simulate the complete physiologic environment, and *in vivo* studies and clinical trials consistently report lack of curcumin toxicity,[11] we expanded our *in vitro* results using an *in vivo* embryonic zebrafish assay.[25] This emerging assay has been used to evaluate toxicity of a broad array of nanoparticles, including other curcumin nanoformulations,[47] offering a more complex analysis compared to cell culture.[48] The highest concentration of 250 ppm evaluated in this study represents a worst case scenario, especially in terms of comparative concentrations in cosmetic products. The experimental duration is from 8 hours post-fertilization, when the embryo consists of only a few cells, to 120 hpf, which is the onset of free feeding.[49] The development of numerous biological processes during this time makes this experimental period a critical and sensitive stage of the animal's life, thereby providing unique insight when studying potential toxicity of an experimental material.

Using the embryonic zebrafish assay to study nanoparticle toxicity can be associated with certain limitations. Nanomaterials are known to agglomerate or settle out of solution if measures are not taken to assure stability. Although these nanomaterials elicited low toxicity in the zebrafish assay, issues of agglomeration and bioavailability need to be considered when interpreting such results. Outside the natural variations in size and body shape of zebrafish,[50] there were no differences in the fish exposed to curc-np compared to untreated control. We maintained background level mortality under 8.3%, below the EPA ecological effects test guideline OPPT5850.1073 of 10%. The model has proven sensitive for studying toxicity of many nanomaterials, including metals and metal oxides, and data for suites of nanomaterials are available on the Nanomaterial-Biological Interactions Knowledgebase (http://nbi.oregonstate.edu).

In summary, curc-np represent a significant advance for the treatment of infected burn wounds, reducing bacterial load and enhancing wound healing. Curc-np technology circumvents the difficulties inherent in curcumin administration, enabling delivery of this therapeutic substance. Unlike currently used treatments, curc-np are less likely to select for resistant bacterial strains or delay wound healing. We conclude that this technology has the potential to serve as a novel topical agent for burn wound infection and possibly other cutaneous injuries.

Supplementary Material

Refer to Web version on PubMed Central for supplementary material.

Acknowledgments

SLH would like to thank the staff of the Sinnhuber Aquatic Research Laboratory (SARL) at Oregon State University.

Funding sources: Dermatology Foundation, Feldstein Medical Foundation, NIH grants ES017552-01A2, ES016896-01, P30 ES000210

References

1. Church D, Elsayed S, Reid O, Winston B, Lindsay R. Burn wound infections. Clin Microbiol Rev. 2006; 19(2):403–434. [PubMed: 16614255]
2. de Macedo JL, Santos JB. Bacterial and fungal colonization of burn wounds. Mem Inst Oswaldo Cruz. 2005; 100(5):535–539. [PubMed: 16184232]
3. Vindenes H, Bjerknes R. Microbial colonization of large wounds. Burns. 1995; 21(8):575–579. [PubMed: 8747728]
4. Aziz Z, Abu SF, Chong NJ. A systematic review of silver-containing dressings and topical silver agents (used with dressings) for burn wounds. Burns. 2012; 38(3):307–318. [PubMed: 22030441]
5. Nguyen TA, Friedman AJ. Curcumin: a novel treatment for skin-related disorders. J Drugs Dermatol. 2013; 12(10):1131–1137. [PubMed: 24085048]
6. Anand P, Sundaram C, Jhurani S, Kunnumakkara AB, Aggarwal BB. Curcumin and cancer: an “old-age” disease with an “age-old” solution. Cancer Lett. 2008; 267(1):133–164. [PubMed: 18462866]
7. Gunes H, Gulen D, Mutlu R, Gumus A, Tas T, Eren Topkaya A. Antibacterial effects of curcumin: an in vitro minimum inhibitory concentration study. Toxicol Ind Health. 2013
8. Sandur SK, Ichikawa H, Pandey MK, Kunnumakkara AB, Sung B, Sethi G, et al. Role of pro-oxidants and antioxidants in the anti-inflammatory and apoptotic effects of curcumin (diferuloylmethane). Free Radic Biol Med. 2007; 43(4):568–580. [PubMed: 17640567]
9. Somparn P, Phisalaphong C, Nakornchai S, Unchern S, Morales NP. Comparative antioxidant activities of curcumin and its demethoxy and hydrogenated derivatives. Biol Pharm Bull. 2007; 30(1):74–78. [PubMed: 17202663]
10. Kulac M, Aktas C, Tulubas F, Uygur R, Kanter M, Erboga M, et al. The effects of topical treatment with curcumin on burn wound healing in rats. J Mol Histol. 2013; 44(1):83–90. [PubMed: 23054142]
11. Gupta SC, Patchva S, Aggarwal BB. Therapeutic roles of curcumin: lessons learned from clinical trials. AAPS J. 2013; 15(1):195–218. [PubMed: 23143785]
12. Flora G, Gupta D, Tiwari A. Nanocurcumin: a promising therapeutic advancement over native curcumin. Crit Rev Ther Drug Carrier Syst. 2013; 30(4):331–368. [PubMed: 23662605]
13. Chereddy KK, Coco R, Memvanga PB, Ucakar B, des Rieux A, Vandermeulen G, et al. Combined effect of PLGA and curcumin on wound healing activity. J Control Release. 2013; 171(2):208–215. [PubMed: 23891622]
14. Bhawana, Basniwal RK, Buttar HS, Jain VK, Jain N. Curcumin nanoparticles: preparation, characterization, and antimicrobial study. J Agric Food Chem. 2011; 59(5):2056–2061. [PubMed: 21322563]
15. Friedman AJ, Han G, Navati MS, Chacko M, Gunther L, Alfieri A, et al. Sustained release nitric oxide releasing nanoparticles: characterization of a novel delivery platform based on nitrite containing hydrogel/glass composites. Nitric Oxide. 2008; 19(1):12–20. [PubMed: 18457680]
16. Seleem MN, Munusamy P, Ranjan A, Alqublan H, Pickrell G, Sriranganathan N. Silica-antibiotic hybrid nanoparticles for targeting intracellular pathogens. Antimicrob Agents Chemother. 2009; 53(10):4270–4274. [PubMed: 19667284]
17. Gupta R, Kumar A. Bioactive materials for biomedical applications using sol–gel technology. Biomed Mater. 2008; 3(3):034005. [PubMed: 18689920]
18. Yuan H, Bao X, Du YZ, You J, Hu FQ. Preparation and evaluation of SiO2-deposited stearic acid-g-chitosan nanoparticles for doxorubicin delivery. Int J Nanomedicine. 2012; 7:5119. [PubMed: 23055724]
19. Martinez LR, Han G, Chacko M, Mihu MR, Jacobson M, Gialanella P, et al. Antimicrobial and healing efficacy of sustained release nitric oxide nanoparticles against Staphylococcus aureus skin infection. J Invest Dermatol. 2009; 129(10):2463–2469. [PubMed: 19387479]

20. Sanchez DA, Schairer D, Tuckman-Vernon C, Chouake J, Kutner A, Makdisi J, et al. Amphotericin B releasing nanoparticle topical treatment of Candida spp. in the setting of a burn wound. Nanomedicine. 2014; 10(1):269–277. [PubMed: 23770066]
21. Han G, Tar M, Kuppam DS, Friedman A, Melman A, Friedman J, et al. Nanoparticles as a novel delivery vehicle for therapeutics targeting erectile dysfunction. J Sex Med. 2010; 7(1 Pt 1):224–233. [PubMed: 19765204]
22. Nacharaju P, Tuckman-Vernon C, Maier KE, Chouake J, Friedman A, Cabrales P, et al. A nanoparticle delivery vehicle for S-nitroso-N-acetyl cysteine: sustained vascular response. Nitric Oxide. 2012; 27(3):150–160. [PubMed: 22705913]
23. Han G, Martinez LR, Mihu MR, Friedman AJ, Friedman JM, Nosanchuk JD. Nitric oxide releasing nanoparticles are therapeutic for Staphylococcus aureus abscesses in a murine model of infection. PLoS One. 2009; 4(11):e7804. [PubMed: 19915659]
24. Altman SA, Randers L, Rao G. Comparison of trypan blue dye exclusion and fluorometric assays for mammalian cell viability determinations. Biotechnol Prog. 1993; 9(6):671–674. [PubMed: 7764357]
25. Truong L, Harper SL, Tanguay RL. Evaluation of embryotoxicity using the zebrafish model. Methods Mol Biol. 2011; 691:271–279. [PubMed: 20972759]
26. Friedman A, Blecher K, Sanchez D, Tuckman-Vernon C, Gialanella P, Friedman JM, et al. Susceptibility of Gram-positive and -negative bacteria to novel nitric oxide-releasing nanoparticle technology. Virulence. 2011; 2(3):217–221. [PubMed: 21577055]
27. Verallo-Rowell VM, Dillague KM, Syah-Tjundawan BS. Novel antibacterial and emollient effects of coconut and virgin olive oils in adult atopic dermatitis. Dermatitis. 2008; 19(6):308–315. [PubMed: 19134433]
28. Wang Y, Lu Z, Wu H, Lv F. Study on the antibiotic activity of microcapsule curcumin against foodborne pathogens. Int J Food Microbiol. 2009; 136(1):71–74. [PubMed: 19775769]
29. Mohanty C, Das M, Sahoo SK. Sustained wound healing activity of curcumin loaded oleic acid based polymeric bandage in a rat model. Mol Pharm. 2012; 9(10):2801–2811. [PubMed: 22946786]
30. Li Q, Frank M, Thisse CI, Thisse BV, Uitto J. Zebrafish: a model system to study heritable skin diseases. J Invest Dermatol. 2011; 131(3):565–571. [PubMed: 21191402]
31. Shehzad A, Lee YS. Molecular mechanisms of curcumin action: signal transduction. Biofactors. 2013; 39(1):27–36. [PubMed: 23303697]
32. Rai D, Singh JK, Roy N, Panda D. Curcumin inhibits FtsZ assembly: an attractive mechanism for its antibacterial activity. Biochem J. 2008; 410(1):147–155. [PubMed: 17953519]
33. Park BS, Kim JG, Kim MR, Lee SE, Takeoka GR, Oh KB, et al. Curcuma longa L. constituents inhibit sortase A and Staphylococcus aureus cell adhesion to fibronectin. J Agric Food Chem. 2005; 53(23):9005–9009. [PubMed: 16277395]
34. Rudrappa T, Bais HP. Curcumin, a known phenolic from Curcuma longa, attenuates the virulence of Pseudomonas aeruginosa PAO1 in whole plant and animal pathogenicity models. J Agric Food Chem. 2008; 56(6):1955–1962. [PubMed: 18284200]
35. Sidhu GS, Singh AK, Thaloor D, Banaudha KK, Patnaik GK, Srimal RC, et al. Enhancement of wound healing by curcumin in animals. Wound Repair Regen. 1998; 6(2):167–177. [PubMed: 9776860]
36. Mani H, Sidhu GS, Kumari R, Gaddipati JP, Seth P, Maheshwari RK. Curcumin differentially regulates TGF-beta1, its receptors and nitric oxide synthase during impaired wound healing. Biofactors. 2002; 16(1-2):29–43. [PubMed: 12515914]
37. Gopinath D, Ahmed MR, Gomathi K, Chitra K, Sehgal PK, Jayakumar R. Dermal wound healing processes with curcumin incorporated collagen films. Biomaterials. 2004; 25(10):1911–1917. [PubMed: 14738855]
38. Cheppudira B, Fowler M, McGhee L, Greer A, Mares A, Petz L, et al. Curcumin: a novel therapeutic for burn pain and wound healing. Expert Opin Investig Drugs. 2013; 22(10):1295–1303.

39. Topman G, Lin FH, Gefen A. The natural medications for wound healing - Curcumin, Aloe-Vera and Ginger - do not induce a significant effect on the migration kinematics of cultured fibroblasts. J Biomech. 2013; 46(1):170–174. [PubMed: 23084784]
40. Prow TW, Grice JE, Lin LL, Faye R, Butler M, Becker W, et al. Nanoparticles and microparticles for skin drug delivery. Adv Drug Deliver Rev. 2011; 63(6):470–491.
41. Samberg ME, Oldenburg SJ, Monteiro-Riviere NA. Evaluation of silver nanoparticle toxicity in skin in vivo and keratinocytes in vitro. Environ Health Perspect. 2010; 118(3)
42. Syng-ai C, Kumari AL, Khar A. Effect of curcumin on normal and tumor cells: role of glutathione and bcl-2. Mol Cancer Ther. 2004; 3(9):1101–1108. [PubMed: 15367704]
43. Anitha A, Deepagan V, Divya Rani V, Menon D, Nair S, Jayakumar R. Preparation, characterization, in vitro drug release and biological studies of curcumin loaded dextran sulphate–chitosan nanoparticles. Carbohydrate Polymers. 2011; 84(3):1158–1164.
44. Kunwar A, Barik A, Mishra B, Rathinasamy K, Pandey R, Priyadarsini K. Quantitative cellular uptake, localization and cytotoxicity of curcumin in normal and tumor cells. Biochim Biophys Acta. 2008; 1780(4):673–679. [PubMed: 18178166]
45. Sanoj Rejinold N, Sreerekha P, Chennazhi K, Nair S, Jayakumar R. Biocompatible, biodegradable and thermo-sensitive chitosan-g-poly (N-isopropylacrylamide) nanocarrier for curcumin drug delivery. Int J Biol Macromol. 2011; 49(2):161–172. [PubMed: 21536066]
46. Arunraj T, Rejinold NS, Mangalathillam S, Saroj S, Biswas R, Jayakumar R. Synthesis, Characterization and Biological Activities of Curcumin Nanospheres. J Biomed Nanotechnol. 2014; 10(2):238–250. [PubMed: 24738332]
47. Kumar SSD, Surianarayanan M, Vijayaraghavan R, Mandal AB, MacFarlane D. Curcumin loaded poly (2-hydroxyethyl methacrylate) nanoparticles from gelled ionic liquid – In vitro cytotoxicity and anti-cancer activity in SKOV-3 cells. Eur J Pharm Sci. 2014; 51:34–44. [PubMed: 24012589]
48. Rizzo LY, Golombek SK, Mertens ME, Pan Y, Laaf D, Broda J, et al. In vivo nanotoxicity testing using the zebrafish embryo assay. J Mater Chem B Mater Biol Med. 2013; 1(32):3918–3925.
49. Strahle U, Scholz S, Geisler R, Greiner P, Hollert H, Rastegar S, et al. Zebrafish embryos as an alternative to animal experiments--a commentary on the definition of the onset of protected life stages in animal welfare regulations. Reprod Toxicol. 2012; 33(2):128–132. [PubMed: 21726626]
50. Irmler I, Schmidt K, Starck JM. Developmental variability during early embryonic development of zebra fish, Danio rerio. J Exp Zool B Mol Dev Evol. 2004; 302(5):446–457. [PubMed: 15580642]

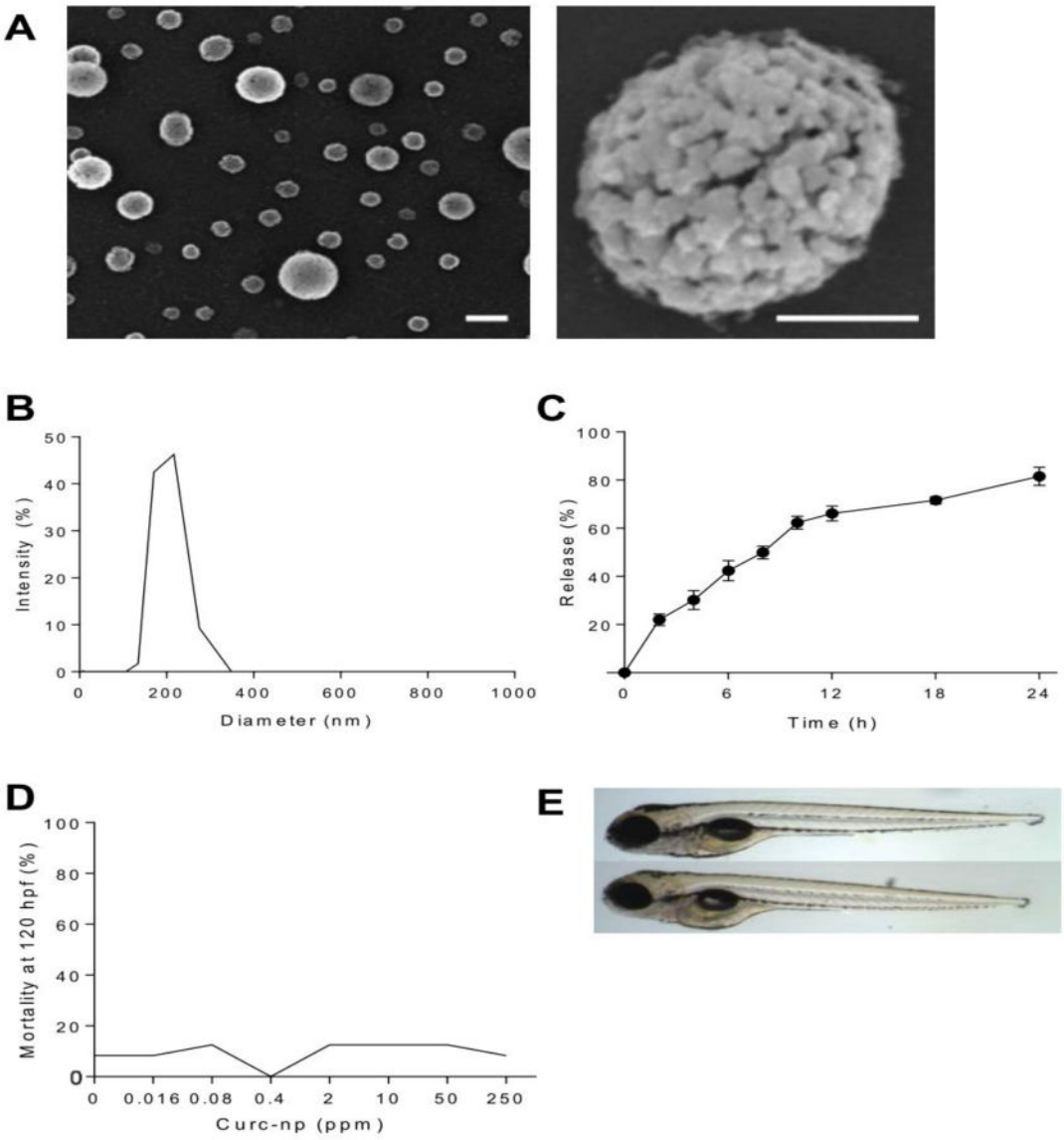

Figure 1. Characterization and toxicity of curc-np

(A) Scanning electron microscopy revealed distinct spherical nanoparticles (left bar=200 nm, right bar=100 nm). (B) Monomodal size distribution quantified by dynamic light scattering indicated a narrow size range with average diameter 222 ± 14 nm. (C) Release occurred in controlled and sustained fashion, reaching 81.5% after 24 hours. (D) Percent mortality at 120 hours post-fertilization (hpf) as a function of exposure concentration. Mortality was not significant for embryos exposed to curc-np compared to fish water control. (E) Representative images of zebrafish embryos at 120 hpf: control (top) and exposed to curc-np (bottom). No significant differences were observed in larval morphology or behavioral endpoints ($p>0.05$ for each endpoint evaluated, Fisher's Exact test). Error bars denote SEM.

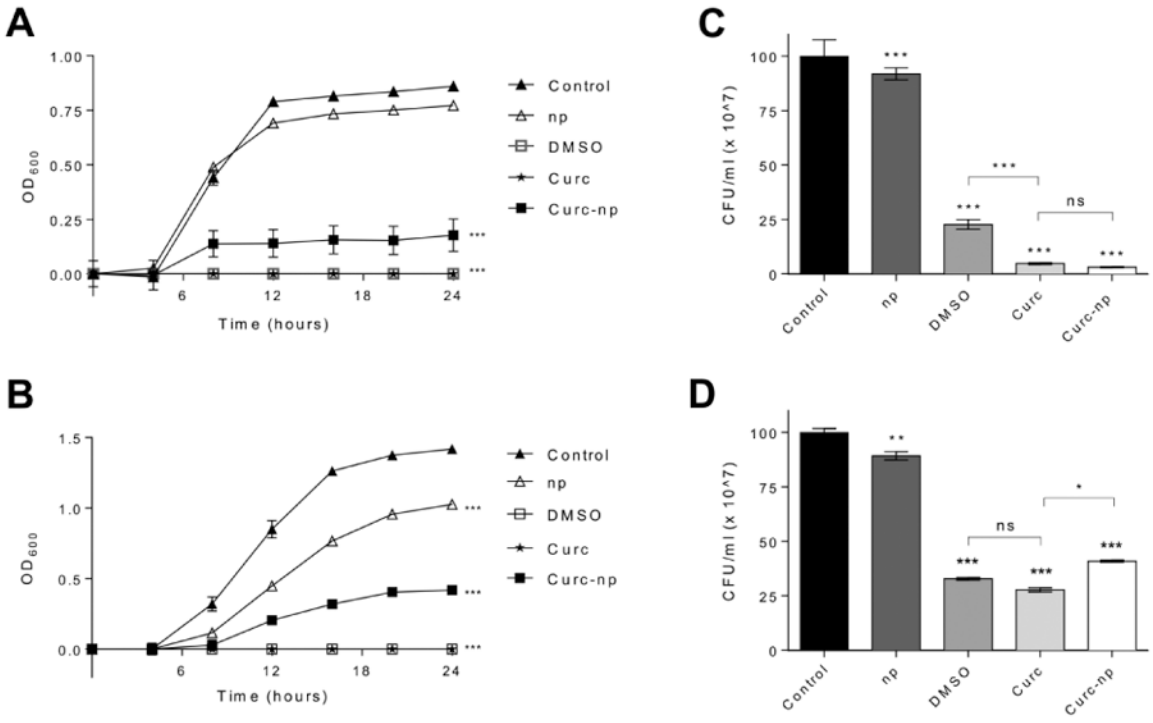

Figure 2. Curc-np inhibit planktonic growth of Gram-positive and -negative organisms

Representative 24-hour growth curves demonstrate susceptibility of (A) MRSA isolates (n=8) and (B) *P. aeruginosa* isolates (n=4) to control np 5 mg/ml (np), 4% DMSO control, curcumin 50 μg/ml in 4% DMSO (curc), and curc-np 5 mg/ml. Colony forming unit (CFU) quantification was performed on (C) MRSA and (D) *P. aeruginosa* isolates to determine antimicrobial activity of these treatment groups. All treatments were performed in triplicate. Statistical analysis conducted using 1-way and 2-way ANOVA. Error bars denote SEM. *** $p \leq 0.0001$, ** $p \leq 0.01$, * $p \leq 0.05$, ns $p > 0.05$.

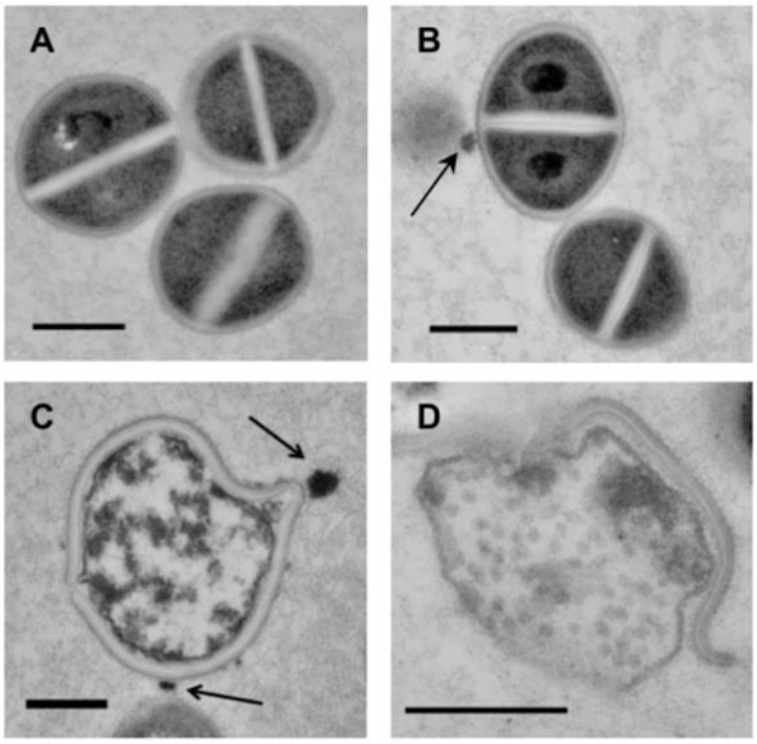

Figure 3. Curc-np induce cellular damage of MRSA

High-power transmission electron microscopy demonstrated interaction of nanoparticles (arrows) with MRSA cells. (A) Untreated MRSA showed uniform cytoplasmic density and central cross wall surrounding a highly contrasting splitting system. (B) After 24 hours, cells incubated with control np 5 mg/ml did not exhibit changes in cellular morphology compared to untreated control. (C) After 6 hours, cells incubated with curc-np 5 mg/ml exhibited distortion of cellular architecture and edema, followed by lysis and extrusion of cytoplasmic contents after 24 hours (D). All scale bars=500 nm.

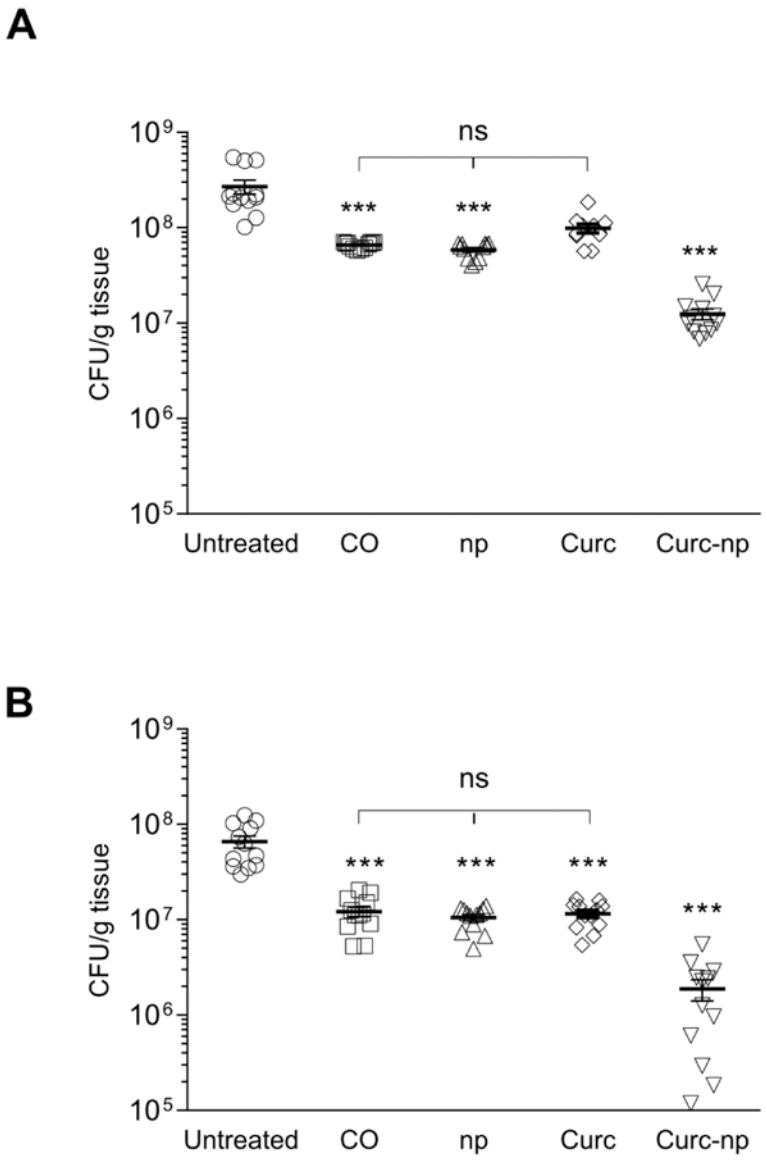

Figure 4. Curc-np decrease bacterial burden of full-thickness burns

Wound bacterial burden (CFU; colony forming unit) in mice infected intradermally with 5×10^8 MRSA cells was determined by amount of CFU growth (n=10 wounds per group). On day 3 (A) and day 7 (B) after infection, bacterial burden of curc-np-treated wounds was significantly lower than untreated, coconut oil (CO), control np (np), and curcumin (curc)-treated wounds. Statistical analysis conducted using 1-way ANOVA. Error bars denote SEM. *** $p \leq 0.001$, ns $p > 0.05$.

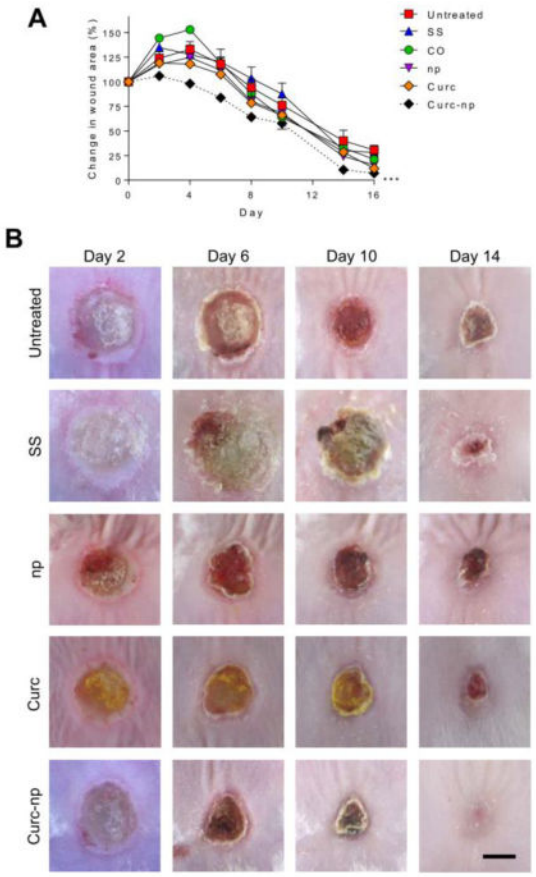

Figure 5. Curc-np accelerate wound healing in a murine burn model

(A) Wound size analysis (relative area versus initial area) revealed statistically significant acceleration of wound healing in mice treated with curc-np compared to untreated, silver sulfadiazine (SS), coconut oil control (CO), control np (np), and curcumin (curc). Time points are averages of 10 measurements. Statistical analysis conducted using 2-way ANOVA. Error bars denote SEM. *** $p \leq 0.0001$. (B) Representative images of wound healing from days 2-14. Topical administration of curc-np decreased eschar size and qualitatively accelerated healing compared to all other groups. CO (vehicle) control did not differ significantly from untreated control (data not shown). Scale bar=5 mm.

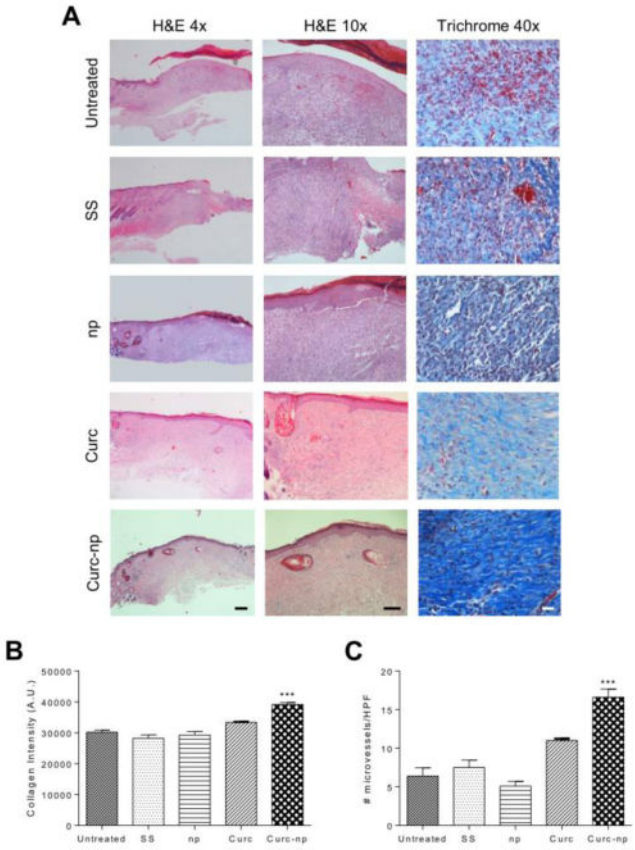

Figure 6. Curc-np enhance formation of granulation tissue, collagen deposition and neoangiogenesis

(A) Histologic analysis of wound tissue from day 13 using hematoxylin and eosin (H&E) and Masson's trichrome staining. On H&E (magnification 4×, bar=500 μm; 10 ×, bar=100 μm), untreated control, silver sulfadiazine (SS) and control np (np)-treated wounds exhibited fibrinous debris and inflammatory granulation tissue compared to accelerated maturation of curc-np-treated wounds. Curcumin (curc) control wounds displayed more dermal inflammation compared to curc-np. On trichrome (magnification 40×, bar=100 μm), increased collagen deposition, more orderly orientation of fibers, and decreased necrosis were appreciated in curc-np-treated wounds compared to all other groups. (B) Quantitative measurement of collagen intensity in 10 representative fields of the same size (in arbitrary units, A.U.). (C) Quantitative measurement of microvessels based on CD34 staining of excised tissue in 10 representative fields of the same size (magnification 40×). Statistical analysis conducted using 1-way ANOVA. Error bars denote SEM. *** $p \leq 0.0001$.